Highly ordered smectic structures of disc-rod luminescent liquid crystals: the role of tolane group

Yurong Liu,[ab] Wei Li,[a] Xuan Zhou,[c] Wai-Yeung Wong*[c] and Zhen-Qiang Yu*[a]

Two novel calamitic tolane luminogen modified triphenylene-based discotic luminescent liquid-crystals (LLC) are rationally designed and synthesized to investigate the self-assembly competition between triphenylene discogens and tolane calamitic mesogens. Results show the LLCs formed thermodynamically stable highly ordered smectic B or smectic E phase as well as the lamellar crystal structures, instead of the traditional columnar phase. The photoluminescence properties depending on their crystal structures are also studied, indicating the important role of tolane group in manipulating the self-organization of disc-rod molecules and consequently achieving enhanced emission.

Introduction

The phase structures and phase transitions of self-assembled organic materials have not only been governing the principles in fundamental science but also formed the basis of material multifunctionalities.[1–4] Engineering molecular self-assembly on nanometer or micron scale is an important approach to tailor solid-state microstructures and develop new functional materials.[5–7] The self-assembly behavior of the classical discogen triphenylene has been a resurgence of research with the current development of nanoscience particularly in thermo- or electro conducting systems.[8–14] Due to the largely π-conjugated planar structure, the self-organized nanostructures of triphenylene based molecules are usually limited to hexagonal or rectangular columnar structures dominated by the strong π-π interactions between the π-conjugated planar discogens.[15] Efforts have been devoted to manipulating the self-assembling of the discotic liquid crystalline (DLC) molecules.[16,17] Apart from constructing hierarchical structures over keeping the columnar structure, breaking the disc packing is another approach to vary the self-organized structures.[18] It has been reported that taking the advantages of the steric hindrance effect, modifying the triphenylene with bulky groups could achieve nematic phase.[19] When six cyanobiphenyl calamitic mesogens were chemically linked to the periphery of the triphenylene discogen through twelve methylene units, benefiting from the decoupling of the two components (rod and disc mesogens), the resultant molecule can form a biaxial nematic phase with the optical director of cyanobiphenyl group orthogonal to the discotic mesogen.[20,21] Besides, introducing rodlike mesogens to the periphery of discotic skeleton through rational selection of the spacer and regulating the interactions between triphenylene mesogens and between the pending calamitic mesogens, also can be a promising dual-component strategy. Shape-induced phase segregation of disc-rod molecules has been studied to form smectic A (SmA) or smectic C (SmC) phase.[22,23] In addition, triphenylene modified with rod-shaped photo-isomerized peripheries have been reported to show thermal- and photoinduced phase transitions and could exhibit thermodynamically metastable SmA state.[24–26] However, to the best of our knowledge, the thermo-dynamically stable, highly ordered smectic phase has never been reported yet.

In this communication, we designed and synthesized two discotic LCs with six tolane mesogenic groups attached to 2,3,6,7,10,11 positions of triphenylene and the name can be abbreviated as **DR-5** and **DR-7** (hereafter collectively called **DR**s, D means discotic triphenylene group, R stands for rodlike tolane mesogenic group, 5 or 7 is the alkyl tail length), and such study is able to illustrate the effective strategy towards thermodynamically stable, functional highly ordered smectic nanostructures. That is, this can trigger the competition between packing of rods and discs by elaborately designing the spacers and rod periphery. The resultant LLCs bear novelty not only with regard to the formed thermodynamically stable highly ordered smectic phase structures but also for the synergistic effect of rod and disc to achieve enhanced luminescence. This study sheds new light into the role of tolane as mesogen and luminogen in disc-rod molecules.

Results and discussion

2.1 Structural design

[a] *School of Chemistry and Environmental Engineering, Low-Dimensional Materials Genome Initiative, Shenzhen University, Shenzhen 518071, China.*
[b] *Department of Chemistry and Materials Science, University of Science and Technology of China, Hefei, 230026 China.*
[c] *Department of Applied Biology and Chemical Technology, The Hong Kong Polytechnic University, Hung Hom, Hong Kong, China and The Hong Kong Polytechnic University Shenzhen Research Institute, Shenzhen Virtual University Park, Nanshan district, Shenzhen 518057, China.*

Chemical structures of **DR-5** and **DR-7** are displayed in Fig. 1. The six tolane mesogens are covalently linked to triphenylene core through six-methylene units. Here the six-methylene spacer plays a very crucial impact on the coupling of dynamics of the two mesogens. Moreover, tolane also could act as a luminogen to achieve versatile functions.[27,28] And the alkyl tail length shows an influence on the molecular mesophase behavior as we earlier demonstrated.[29,30] The target molecules are prepared by the route depicted in Scheme S1. The tolane groups are embedded into the skeleton of triphenylene by the nucleophilic substitution reaction of hexahydroxytriphenylene (**10**) with **R-5** and **R-7** (hereafter collectively called **R**s), respectively. It was found that the collected powder **DR**s are blue emissive as shown in Fig. 1. The phase behaviors are investigated by differential scanning calorimetry (DSC), polarized optical microscopy (POM) and temperature dependent wide-angle X-ray diffraction (WAXD). Interestingly, the **DR**s can form stable highly ordered smectic phase, instead of traditional columnar structure due to the overwhelming strong interaction between tolanes over the interaction between the triphenylene rings.

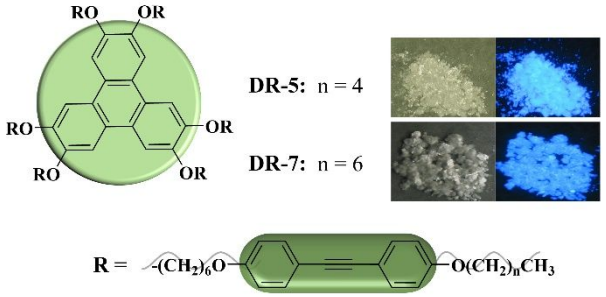

Fig. 1. Chemical structures of **DR-5** and **DR-7** (the structures of triphenylene and tolane are respectively modelled as disc and rod) and the photographs of them in solid-state under sunlight and UV light, respectively.

2.2 Characterization

DSC trace of **DR-5** (Fig. 2a) shows three exothermic peaks at 65 °C, 57 °C and 35 °C on cooling at a scan rate of 5 °C min^{-1}, whereas only one endothermic peak at 72 °C is recorded on heating, implying the monotropic LC transition. The transition at 35 °C could be assigned to LC to crystal transition. The other two transitions at 57 °C and 65 °C are associated with the transitions of LC-LC and LC-isotropic phases. Interestingly, **DR-7**, with similar chemical structure to **DR-5**, exhibits a quite different phase transition behavior. Two sets of peaks are detected during cooling and subsequent heating cycles, suggesting the enantiotropic nature of **DR-7**. The transition temperature at 75 °C during cooling is very close to that at 77 °C during heating, indicating a thermodynamic equilibrium, which is associated with LC phase transitions.[31] In contrast, the transition at lower temperature shows supercooling of 15 °C, which could be assigned to the LC-crystal phase transition. The POM was applied to observe the textures of **DR**s. When observed under POM, **DR-5** shows a focal conic texture (Fig. 2b and Fig. S1) upon cooling from the isotropic liquid to 63 °C, indicative of the smectic mesophase formation. By continuing cooling down to 55 °C, another focal conic texture was observed, reflecting that another smectic phase or other very similar phase was formed. By further lowering the temperature, the crystallization occurs. For **DR-7**, the POM microphotograph also clearly depicts the emerged focal conic texture in both heating and cooling procedure at 75 °C as shown in Fig. 2b and Fig. S1. The POM observations are consistent with their corresponding DSC results, confirming the LC phase transitions. The difference in phase transition behaviors between **DR**s implies that the minor disparity in alkyl tail lengths could exert a strong effect on the molecular packing behavior.

WAXD was performed to get insights into the molecular packing in different mesophases. Fig. 2c shows the diffraction patterns of **DR**s at LC state collected upon cooling from isotropic melts. For **DR-5**, when cooled to 60 °C, a very strong and a very weak peak at 2θ of 2.89° and 5.76° with a *d*-spacing ratio of 1:1/2 are collected in the low-angle region, indicating a layered structure with a layer thickness of 3.06 nm, while in the wide- angle region, a sharp and intense reflection at 2θ of 20.6° with a *d*-spacing of 0.43 nm and a broad scattering halo centered at around 20° were detected. It unveils the long-range ordered packing of tolane groups on sub-nanometer scale and the amorphous packing of the alkyl tails, indicative of a smectic B (SmB) phase of **DR-5** rather than hexatic B phase which only shows short-range ordering on sub-nanometer scale.[32] By further cooling to 50 °C, three reflections with a *d*-spacing ratio of 1:1/2:1/3 are detected in the low-angle region, clearly rendering a highly ordered smectic LC phase with a layer thickness of 1.87 nm. Two fresh reflections at 2θ of 23.58° and 25.35° in high-angle region emerged, which is highly reminiscent of the birth of a smectic E (SmE) phase, suggesting the hexagonally packed molecular packing model of tolane groups on the sub-nanometer scale transformed to a rectangular one.[33–35] The three peaks labeled to 1', 2' and 3' can be assigned as (110) (200) and (210) diffractions of the SmE phase on sub-nanometer scale with a' = 0.75 nm, b' = 0.54 nm and γ = 90°. Therefore, the average area occupied by each tolane group of **DR-5** in the $a'b'$ plane is around 0.20 nm^2 (i.e., $a'b'/2$), matching the reported value well.[34–36] The sharpness of the reflections 1 and 1' respectively illuminates the long-range correlation of the interlayer and intralayer orders. It is also noted that the sharp peak at 57 °C detected during DSC trace is commonly associated to the mesophase with high degree of orders.[17] The DSC data offers further support upon the WAXD analysis. Briefly, **DR-5** can sequentially form SmB and SmE phases before crystallization with the layer thickness of 3.06 nm in SmB phase much larger than that of 1.87 nm in SmE phase. By contrast, **DR-7** also exhibits a smectic B phase when cooled to 75 °C, but the reflection 1 shifts to lower angle region with the lamellae thickness 0.3 nm thicker than that of **DR-5**, which is about the extended length of four methylene units, indicating that the alkyl tails take extended conformation and dominate the lamellae thickness. Besides, **DR-7** forms enantiotropic LC phase

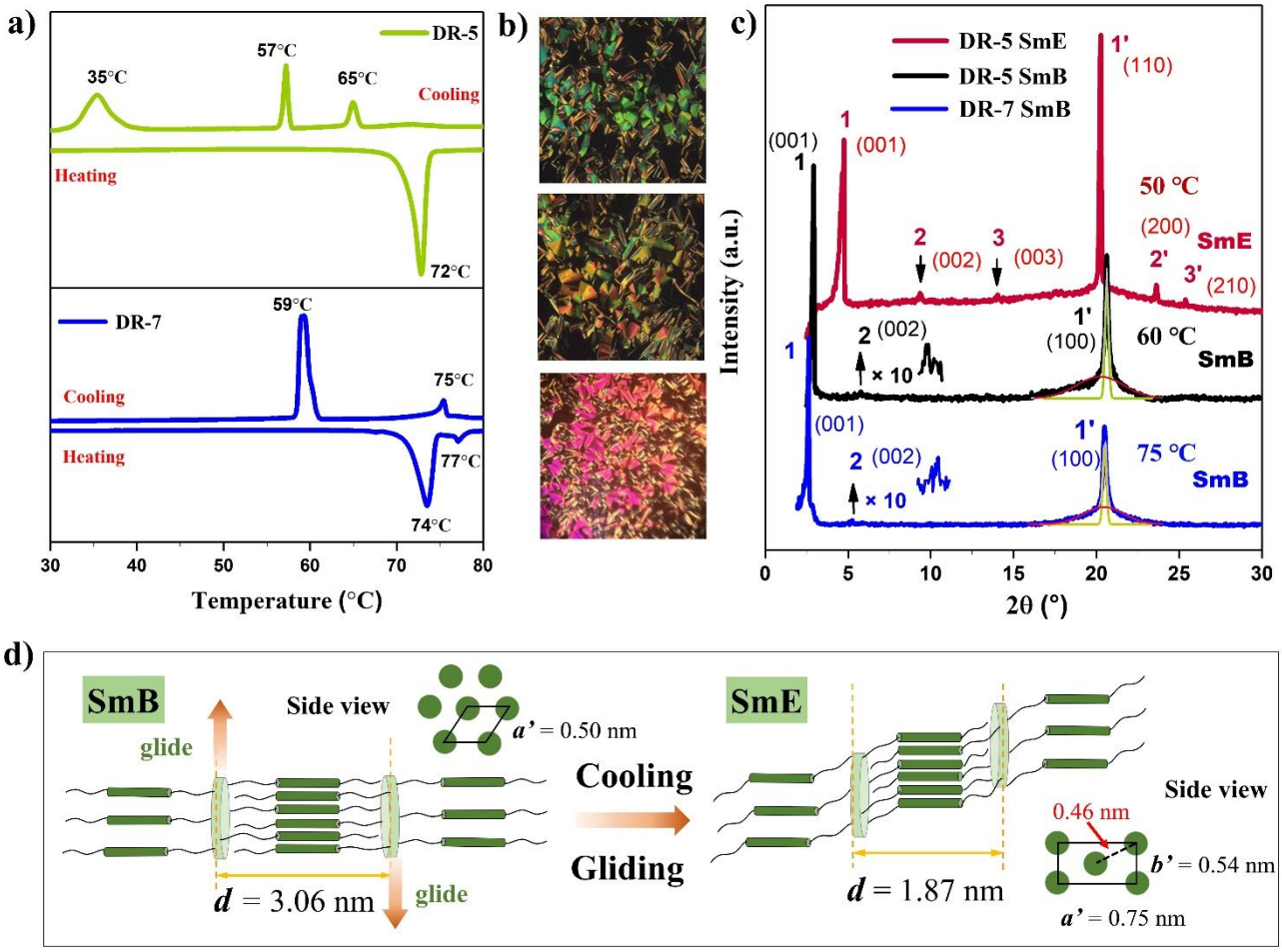

Fig. 2. a) DSC traces of **DR**s detected upon cooling and subsequent heating with a scan rate of 5 °C·min^{-1}. b) POM textures of **DR-5** observed at 63 °C (up), 55 °C (middle) and that of **DR-7** at 75 °C (down) upon cooling from isotropic melts with a cooling speed of 1°C·min^{-1}. c) The WAXD patterns of **DR**s at different mesophases. d) Schematic illustration of the molecular packing models of **DR-5** in SmB and SmE phase and the side views of the models along the tolane mesogens.

and the SmB phase cannot be further developed into SmE phase during cooling. These phenomena indicate that the phase structures are partially dependent on the alkyl tail length. It is also worth noting that the characteristic diffraction at 2θ of ~25° of the ordered face-on stacking of triphenylene discogen through intermolecular π-π interaction is absent in both WAXD patterns of SmB and SmE phase of **DR-5**, indicating that the SmB-SmE transition can be assigned to a further ordering of the tolanes. These observations strongly suggest that the tolane mesogens preferentially bundle to form a layer and dominate the molecular packing structure. In the meanwhile, the traditional ordered packing between triphenylene discogens is hindered.

What is the driving force of these different molecular packing models? It may include molecular shape and spacing filling effects. Based on the above analysis, the proposed molecular packing models for **DR-5** are schematized in Fig. 2d. The peripheral tolane groups are alternately assigned on both sides of the triphenylene plane and aligned to give a layered phase structure. In both molecular packing models, the tolane groups take interdigitated packing manner. When the temperature decreased, the *d*-spacing on the nanometer or sub-nanometer scale will be slightly shrunken, but the lateral shrinkage ratio in the tolane region and alkyl tail region is different: the loosely packed alkyl tail region will be squeezed by the closely packed tolane region, and the different shrinkage ratio of different region will lead to slightly gliding of the tolane

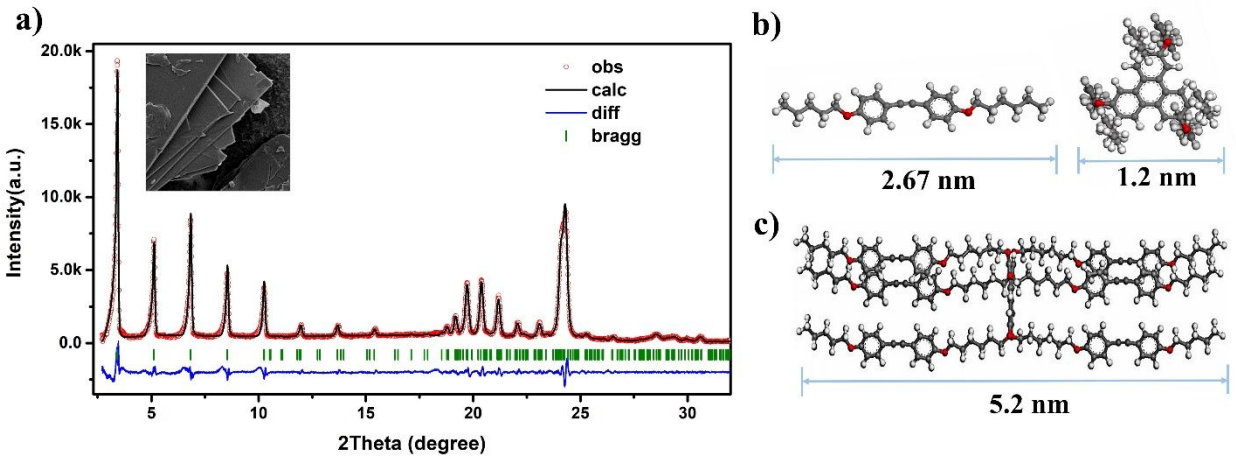

Fig. 3. a) The refinement of powder WAXD pattern of **DR-5** in crystal phase. The inset is the corresponding SEM morphology. The observed and the calculated profile perfectly overlapped, and the difference plot shown at the bottom is also very small. The calculated molecular sizes of b) tolane motif (containing the spacer and alkyl tail) (left) as well as triphenylene core (right) and c) **DR-5**.

region along the lateral direction. This slight lateral glide decreases the layer thickness on the one hand and on the other hand changes the packing model of tolane group from two-dimensional hexagonal lattice to the rectangular one.

2.3 Self-assembly of the disc-rod molecules

The self-assembly of **DR**s in crystal phase was further investigated. Inset of Fig. 3a shows the scanning electron microscopy (SEM) layered morphology of **DR-5** prepared from solvent evaporation of THF solution, indicating the layered structure in crystal phase. Sheet-like morphology with large domain sizes are unveiled for both **DR**s and **R**s (Fig. S2). In contrast, methoxy or hydroxy substituted triphenylene compounds **9** and **10**, as referential molecules, disclose distinct bulk morphologies, which should be attributed to the π-π stacking of the triphenylene cores. Fig. 3a and S4a show the powder WAXD patterns of **DR-5** and **DR-7** in crystal state, respectively. The reflections in small-angle region of **DR-5** with a *d*-spacing ratio of 1/2:1/3:1/4:1/5:1/6:1/7:1/8:1/9 and the multi reflections in wide-angle region confirm the prominent layered crystal structure, implying the further ordering of the dominated rods from LC phases. The lamellar structures of **R**s are also revealed in Fig. S3, which is in accordance with the SEM images. The low-angle diffraction patterns of **R**s are very similar to that of **DR**s, which can be considered for the indication of the governance of tolane groups in the self-organization of **DR**s. And their difference in wide-angle region describes the effect of the triphenylene core on guiding molecular packing. Because it is very difficult to obtain suitable single crystals of **DR**s to conduct single crystal diffraction study, structural refinement was applied to get the crystal structure of **DR**s. The refinement data discloses two monoclinic systems ($P2_1/c$ space group) with a = 5.2 nm, b = 0.48 nm and c = 1.7 nm ($\alpha = \gamma = 90°$ and β = 94.3°) for **DR-5** and a = 5.6 nm, b = 0.48 nm and c = 1.7 nm ($\alpha = \gamma = 90°$ and β = 93.5°) for **DR-7** (Table S1 and Fig. S5). Increasing the tail length leads to the increase of a dimension of the unit cell, but no change on the b and c dimensions, suggesting the alkyl tails as well as tolane groups and spacers are orientated along with a-axis. Meanwhile, longer tail also gives rise to larger layer thickness of smectic phase as aforementioned. The formed lamella should stack in parallel to bc plane and subsequently perpendicular to the orientation of the tolane groups. Assuming that all the spacers and alkyl tails take all-*trans* conformation, the molecular sizes of both core and tolane components are calculated out *via* geometrical optimization method by density functional theory (DFT). The tolane motif (containing the spacer and alkyl tail) for **DR-5** shows a length of around 2.67 nm while the discotic core exhibits a diameter of around 1.2 nm (that is D value) (Fig. 3b). Then the molecular length of **DR-5** (Fig. 3c) is calculated to be 5.2 nm (5.7 nm for **DR-7**), well matching the a dimensions of the corresponding unit cells. The b dimension of the unit cell (0.48 nm) is comparable to the lateral distance of the tolane mesogen (0.50 nm in SmB and 0.54 nm in SmE). Hence, the crystal structure of **DR**s can be adopted as the schematic drawing shown in Fig. S4b (viewed along the b axis), wherein the triphenylene cores and tolane groups are respectively modelled as discs and rods, chemically linked through flexible spacers.

Why do **DR**s form highly ordered smectic phase and what role does the tolane mesogen play during the LC phase

formation? There would be a competition on which factor governs the self-assembling between the tolane groups and the triphenylene cores due to the coupling of the dynamics of the two mesogens. But, according to the optimized geometry, the triphenylene core is slightly distorted and the planarity is broken, the interdigitated packing of tolane groups is predominated to form a 2D arrangement parallel to *bc* plane, while the triphenylene discs are intercalated, preventing the π-π stacking of triphenylene-core to form face-on stacked columns. In this context, **DR**s can exhibit ordered smectic LC phases without the co-existence of columnar structure. On the other hand, it was found in our previous study that the tolane-based calamitic LC molecule could form SmC or SmB.[27] Thus, the triphenylene core here may behave as an anchor of tolane mesogens, playing a synergistic effect on the self-assembling of tolane groups to construct a highly ordered smectic phase with additional ordering on the sub-nanometer scale. According to the crystal stacking model, the average area occupied with each tolane group within the discotic plane can be calculated to be $(1/4*\pi D^2)/6 = 0.19$ nm^2 (D is the diameter of triphenylene core), slightly smaller than that in SmB (0.22 nm^2) and SmE (0.20 nm^2) phase and indicative of the close packing of the tolane in crystal state. The proposed stacking model also could provide a reasonable explanation upon the effect of alkyl tail on the packing of tolane groups (as demonstrated in Fig. S4c). For **DR-5**, the spacer is slightly longer than the alkyl tail, accordingly, resulting in almost full contact of tolane groups of the neighboring molecules and subsequently strong interaction between the tolane groups. Increasing the tail length, as in **DR-7**, will lead to less contact and thereby weakened interaction. In this context, compared with **DR-5**, **DR-7** shows a larger layer thickness in SmB phase and cannot be further developed into highly ordered SmE phase, which also may lead to the lower quantum yield compared to **DR-5** (*vide infra*).

2.4 Photoluminescence of the disc-rod molecules

AIE-active LC materials are promising candidates of high-performance luminescent liquid crystals (LLC), as they are completely free of aggregate-caused quenching (ACQ) during fabrication of solid-state device. Therefore, it is interesting to investigate the heredity and variation behavior when embedding the tolane, also a typical AIEgen, into a self-organized system. It was found that **DR**s are non-emissive in solution but emit blue light in solid state under UV illumination, suggesting their AIE activity. The luminescent properties were studied in THF/water mixtures with different water fractions (f_w), where THF is a good solvent and water is a poor solvent for all samples. Taking **DR-5** as an example, the absorption spectrum (Fig. S6a) is not the simple combination of the corresponding moieties **R-5** and **9**. With f_w increasing from 0% to 99%, the emerged fresh peak and enhanced intensity in UV-Vis absorption spectra could be attributed to the scattering effect of in-situ generated nanoaggregates.[37] The recorded photoluminescence (PL) spectra (Fig. S7a-d) also validate that **DR**s and **R**s are AIE active. Besides, the similarity in PL spectra between **DR**s and **R**s indicates that the luminescent properties of **DR**s mainly inherit from the inserted tolane group. The PL intensity at the maximum emission wavelength is boosted by different times upon aggregation: with f_w increasing from of 0% to 99%, the emission enhancement for **DR**s is more obvious than that for **R**s, which can be concluded from Fig. S7e. As tolane groups exhibit crystal-induced emission,[13] the above observation strongly implies that the triphenylene cores have a positive effect on the alignment of peripheral tolane groups to form more ordered molecular stacking instead of disordered nanoaggregates. The noticeable increase in quantum yield (QY) in crystal state provides further evidence on that. The QY of **R-5** with value of 6.9% dramatically increased to 28.5% after the chemical attachment of **R-5** towards triphenylene core to form **DR-5**. The QY value of **DR-7** of 16.3% is much smaller than that of **DR-5**, which may be caused by the less contact of tolane groups during molecular packing. Excitation and absorption spectra are also simulated by time-dependent density functional theory (TD-DFT) using Gaussian at the B3LYP/6-31G(d) level. The obtained computational absorption spectra are displayed in Fig S6c. The calculated maximum absorption wavelength of compound **R** is at around 300 nm, which is close to that of target **DR** but red-shifted compared with compound **9** (~225 nm). Besides, the calculated spectrum of **DR** is not the simple overlay of that of compound **9** and **R**. These results match well with the experimental data. The optimized geometries and the main molecular orbitals involved are shown in Fig. S6d-f. As can be seen, for the components **R**s and compound **10**, both the HOMO and LUMO orbitals are distributed on the whole molecules, indicating the large π-conjugation. In contrast, the HOMO orbital of **DR**s is distributed in the peripheral tolane group while the LUMO orbital is contributed by both the triphenylene core and tolane side substituents. It reveals that the coupling between the two components occurs not only on molecular self-assembling but also in molecular orbital formation, where the tolane moiety shows a dominated effect. The solid-state UV-Vis and PL spectra are plotted in Fig. 4a and b, also depicting the domination of tolane component on the optical properties of **DR**s. The photographs of **DR**s and **R**s recorded during heating and cooling processes under sunlight and UV light are vividly contrasted in Fig. S8 to further illustrate the enhanced photoluminescence of **DR**s caused by the ordered molecular self-organization.

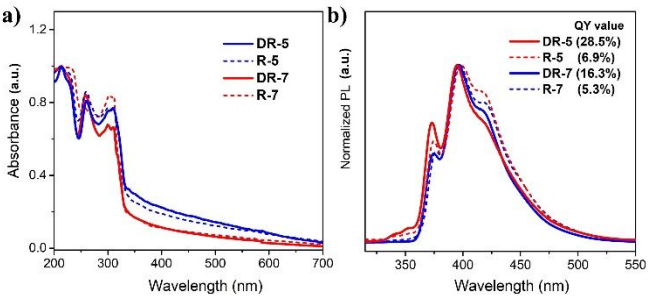

Fig. 4. a) Absorption and b) PL spectra of **DR**s and **R**s in solid-state. The photoluminescence quantum yields of **DR**s and **R**s are indicated in b).

Conclusions

To summarize, through rational modification of the periphery of the discotic triphenylene molecule with calamitic tolane luminogens, two AIE-active LLC materials **DR-5** and **DR-7**, which exhibit desired thermodynamically stable highly ordered smectic phases, are successfully achieved for the first time. The LC phase structures and phase transitions are studied. The sheet-like morphologies are confirmed by SEM images and the lamellar molecular structures are disclosed by WAXD patterns. The absence of the typical columnar stacking of the triphenylene-based discogen occurs in both mesophase and crystal state, as a result of the dominant packing of tolan over the stacking of discotic triphenylene. A stacking model is proposed to satisfy the experimental observations. Taking the advantages of the ordered molecular packing, **DR-5** and **DR-7** exhibit enhanced AIE effect, with respect to the corresponding tolan-based molecules **R-5** and **R-7**. The study presented here evidently illustrates the feasible strategy towards manipulating the molecular self-organization by rationally introducing functional motif and subsequently promoting the performance.

Experimental section

4.1 Synthetic procedures

Synthesis of DR-5. Hexahydroxytriphenylene (0.16 g, 0.4 mmol) and dried KOH (0.25 g, 3.6 mmol) were placed in an oven-dried flask. After three times of pumping and purging with N_2, compound **R-5** (1.42 g, 3.2 mmol) dissolved in 15 mL anhydrous DMF was slowly injected into the mixture. The mixture was heated to 100 ℃ and allowed to react for 72 h. The mixture was poured into 50 mL water and the rude product was filtered and purified by column chromatography afforded the product with a yield of 20%. ^{1}H NMR (400MHz, $CDCl_3$), δ (TMS, ppm)：8.06 (s, 6H), 7.44 (d, *J* = 8.0 Hz, 24H), 6.86 (d, *J* = 8.0 Hz, 24H), 4.19 (t, *J* = 4.0 Hz, 12H), 3.98 (td, *J* = 8.0Hz, 4.0 Hz, 24H), 1.82-1.69 (m, 36H), 1.48-1.35 (m, 48H), 0.93 (t, 18H).^{13}C NMR (400MHz, $CDCl_3$) δ：161.38, 159.13, 133.05, 115.76, 115.42, 114.70, 88.16, 68.27, 67.98, 64.13, 29.20, 28.94, 28.66, 28.39, 25.88, 22.57, 14.28; MALDI-TOF-MS (m/z): $[M+H]^+$ calculated for $C_{168}H_{193}O_{18}$, 2499.4142. found, 2499.4120.

Synthesis of DR-7. DR-7 was synthesized by similar procedures to **DR-5** while compound **R-7** (1.51 g, 3.2 mmol) was used to get a while solid in a yield of 22%. ^{1}H NMR(400MHz, $CDCl_3$), δ(TMS, ppm)：8.05 (d, 6H), 7.43 (d, *J* = 8.0 Hz, 24H), 6.83 (d, *J* = 8.0 Hz, 24H), 4.16 (t, *J* = 4.0 Hz, 12H), 3.94 (td, *J* = 8.0, 4.0 Hz, 24H), 1.81-1.72 (m, 24H), 1.46-1.30 (m, 72H), 0.89 (t, *J* = 8.0 Hz, 18H).^{13}C NMR (400MHz, $CDCl_3$) δ：161.33, 159.09, 133.01, 115.72, 115.70, 114.65, 88.15, 68.23, 67.93, 64.07, 31.97, 29.90, 29.33, 29.30, 28.63, 26.18, 25.85, 22.80, 14.28. MALDI-TOF-MS (m/z): $[M+H]^+$ calculated for $C_{180}H_{217}O_{18}$, 2667.6020; found, 2667.6101.

4.2 Computational simulation

The WAXD refinement profiles were obtained through Le Bail refinement. Computer modelling was conducted to get the data on the molecular size. A single molecule of **DR** containing six tolan groups, one triphenylene core and six alkyl spacers and six alkyl tails was constructed by Materials Studio (Accelrys). We further assumed that the spacers and the alkyl tails were in all *trans* conformation. The geometry optimization was conducted by quantum chemistry method (DFT) using Dmol3 model in Materials Studio. The PW31 model in Generalized Gradient Approximation (GGA) was used for exchange-correlation energy calculation.

To study the optical properties of them, the energy optimization calculation for the tolan group, triphenylene group and the final target compound (named compound **7'**, **9** and **DR'** respectively) were individually conducted. To simplify the calculation, the alkyl spacers and tails were rationally represented by methyl units. Geometry optimization was performed using gaussian D 01 at D 01 at B3LYP/6-31G level while UV-vis absorption spectra were calculated on 30 states using TD-DFT at D 01 at B3LYP/6-31G level.

Conflicts of interest

There are no conflicts to declare.

Acknowledgements

This work was financially supported by National Natural Science Foundation of China (Nos. 21875143, 21674065), Innovation Research Foundation of Shenzhen (Nos. JCYJ20180507182229597 and JCYJ20170817100547775), and the Natural Science Foundation of Guangdong Province (No. 2016A030312002). W.-Y. W. would like to thank the Science, Technology and Innovation Committee of Shenzhen Municipality (JCYJ20180507183413211), the Hong Kong Research Grants Council (PolyU 123384/16P), Hong Kong Polytechnic University (1-ZE1C) and the Endowed Professorship in Energy from Ms. Clarea Au (847S). Y. Liu and X. Zhou would like to thank China Postdoctoral Science Foundation Funded Project (2020M672817 and 2019M653007). The theoretical calculations described in paper were supported by the High-Performance Cluster Computing Centre of Hong Kong Baptist University, which receives funding from the Research Grants Council, University Grants Committee of the HKSAR. Special thanks to the Instrumental Analysis Center of Shenzhen University (Xili Campus).

Notes and references

1 T. Kajitani, K. Motokawa, A. Kosaka, Y. Shoji, R. Haruki, D. Hashizume, T. Hikima, M. Takata, K. Yazawa, K. Morishima, M. Shibayama and T. Fukushima, *Nat. Mater.*, 2019, **18**, 266–272.

2 J. Huang, Z. Su, M. Huang, R. Zhang, J. Wang, X. Feng, R.

Zhang, R. Zhang, W. Shan, X.-Y. Yan, Q.-Y. Guo, T. Liu, Y. Liu, Y. Cui, X. Li, A.-C. Shi and S. Z. D. Cheng, *Angew. Chem. Int. Ed.*, 2020, **59**, 18563–18571.

3 T. Qin, G. Zhou, H. Scheiber, R. E. Bauer, M. Baumgarten, C. E. Anson, E. J. W. List and K. Müllen, *Angew. Chem. Int. Ed.*, 2008, **47**, 8292–8296.

4 T. M. Figueira-Duarte and K. Müllen, *Chem. Rev.*, 2011, **111**, 7260–7314.

5 X. Cheng, T. Miao, L. Yin, Y. Ji, Y. Li, Z. Zhang, W. Zhang and X. Zhu, *Angew. Chem. Int. Ed.*, 2020, **59**, 9669–9677.

6 R. Zhang, X. Feng, R. Zhang, W. Shan, Z. Su, J. Mao, C. Wesdemiotis, J. Huang, X. Yan, T. Liu, T. Li, M. Huang, Z. Lin, A. Shi and S. Z. D. Cheng, *Angew. Chem. Int. Ed.*, 2019, **58**, 11879–11885.

7 B. Shao, S. Wan, C. Yang, J. Shen, Y. Li, H. You, D. Chen, C. Fan, K. Liu and H. Zhang, *Angew. Chem. Int. Ed.*, 2020, **59**, 18213-18217.

8 A. M. van de Craats, J. M. Warman, A. Fechtenkötter, J. D. Brand, M. A. Harbison and K. Müllen, *Adv. Mater.*, 1999, **11**, 1469–1472.

9 L. Zhi and K. Müllen, *J. Mater. Chem.*, 2008, **18**, 1472–1484.

10 D.-G. Kang, M. Park, D.-Y. Kim, M. Goh, N. Kim and K.-U. Jeong, *ACS Appl. Mater. Interfaces*, 2016, **8**, 30492–30501.

11 M. K. Smith and K. A. Mirica, *J. Am. Chem. Soc.*, 2017, **139**, 16759–16767.

12 D. Sheberla, L. Sun, M. a Blood-Forsythe, S. Er, C. R. Wade, C. K. Brozek, A. Aspuru-Guzik and M. Dincă, *J. Am. Chem. Soc.*, 2014, **136**, 8859–8862.

13 T. Kambe, R. Sakamoto, T. Kusamoto, T. Pal, N. Fukui, K. Hoshiko, T. Shimojima, Z. Wang, T. Hirahara, K. Ishizaka, S. Hasegawa, F. Liu and H. Nishihara, *J. Am. Chem. Soc.*, 2014, **136**, 14357–14360.

14 M. G. Campbell, S. F. Liu, T. M. Swager and M. Dincă, *J. Am. Chem. Soc.*, 2015, **137**, 13780–13783.

15 Z.-Q. Yu, J. W. Y. Lam, K. Zhao, C.-Z. Zhu, S. Yang, J.-S. Lin, B. S. Li, J.-H. Liu, E.-Q. Chen and B. Z. Tang, *Polym. Chem.*, 2013, **4**, 996–1005.

16 D. Zeng, I. Tahar-Djebbar, Y. Xiao, F. Kameche, N. Kayunkid, M. Brinkmann, D. Guillon, B. Heinrich, B. Donnio, D. A. Ivanov, E. Lacaze, D. Kreher, F. Mathevet and A.-J. Attias, *Macromolecules*, 2014, **47**, 1715–1731.

17 I. Tahar-djebbar, F. Nekelson, B. Heinrich, B. Donnio, D. Guillon, D. Kreher and F. Mathevet, *Chem. Mater.*, 2011, **23**, 4653–4656.

18 M. Lehmann, M. Hecht, S. Herbst, K. Cui and F. Würthner, *Chem. Commun.*, 2020, **56**, 14015-14018.

19 M. Gupta, S. P. Gupta, M. V. Rasna, D. Adhikari, S. Dhara and S. K. Pal, *Chem. Commun.*, 2017, **53**, 3014–3017.

20 K.-U. Jeong, A. J. Jing, B. Mansdorf, M. J. Graham, D.-K. Yang, F. W. Harris and S. Z. D. Cheng, *Chem. Mater.*, 2007, **19**, 2921–2923.

21 K.-U. Jeong, A. J. Jing, B. Monsdorf, M. J. Graham, F. W. Harris and S. Z. D. Cheng, *J. Phys. Chem. B*, 2007, **111**, 767–777.

22 P. H. J. Kouwer and G. H. Mehl, *Angew. Chem. Int. Ed.*, 2003, **42**, 6015–6018.

23 P. H. J. Kouwer, J. Pourzand and G. H. Mehl, *Chem. Commun.*, 2004, **4**, 66–67.

24 Y. Shimizu, A. Kurobe, H. Monobe, N. Terasawa, K. Kiyohara and K. Uchida, *Chem. Commun.*, 2003, **3**, 1676–1677.

25 D. Tanaka, H. Ishiguro, Y. Shimizu and K. Uchida, *J. Mater. Chem.*, 2012, **22**, 25065–25071.

26 D. Tanaka, H. Ishiguro, T. Shirasu, D. Okuda, K. Uchida and Y. Shimizu, *Mol. Cryst. Liq. Cryst.*, 2014, **594**, 105–111.

27 Y. Chen, J. Lin, W. Yuan, Z.-Q. Yu, J. W. Lam and B. Z. Tang, *Sci. China Chem.*, 2013, **56**, 1191–1196.

28 S.-J. Wang, R.-Y. Zhao, S. Yang, Z.-Q. Yu and E.-Q. Chen, *Chem. Commun.*, 2014, **50**, 8378–8381.

29 Z.-Q. Yu, J. W. Y. Lam, C. Zhu, E. Chen and B. Z. Tang, *Macromolecules*, 2013, **46**, 588–596.

30 Z.-Q. Yu, T.-T. Li, Z. Zhang, J.-H. Liu, W. Z. Yuan, J. W. Y. Lam, S. Yang, E.-Q. Chen and B. Z. Tang, *Macromolecules*, 2015, **48**, 2886–2893.

31 S. Z. D. Cheng, *Phase Transitions in Polymers: The Role of Metastable States*, Elsevier, 2008.

32 S. Paul, B. Ellman, S. Tripathi and R. J. Twieg, *J. Appl. Phys.*, 2015, **118**, 135702.

33 M. Al-Hussein, W. H. de Jeu, L. Vranichar, S. Pispas, N. Hadjichristidis, T. Itoh and J. Watanabe, *Macromolecules*, 2004, **37**, 6401–6407.

34 M. Yamada, A. Hirao, S. Nakahama, T. Iguchi and J. Watanabe, *Macromolecules*, 1995, **28**, 50–58.

35 S.-Y. Park, T. Zhang, L. V Interrante and B. L. Farmer, *Macromolecules*, 2002, **35**, 2776–2783.

36 H. Lou Xie, C. K. Jie, Z. Q. Yu, X. B. Liu, H. L. Zhang, Z. Shen, E. Q. Chen and Q. F. Zhou, *J. Am. Chem. Soc.*, 2010, **132**, 8071–8080.

37 Y. Wu, L. H. You, Z.-Q. Yu, J.-H. Wang, Z. Meng, Y. Liu, X.-S. Li, K. Fu, X.-K. Ren and B. Z. Tang, *ACS Mater. Lett.*, 2020, **2**, 505–510.